Supporting information

Single particle deformation and analysis of silica coated gold nanorods before and after femtosecond laser pulse excitation

Wiebke Albrecht,*,† Tian-Song Deng,† Bart Goris,‡ Marijn A. van Huis,†
Sara Bals,‡ and Alfons van Blaaderen*,†

† *Soft Condensed Matter, Debye Institute for Nanomaterials Science, Utrecht University, Princetonplein 5, 3584 CC Utrecht, The Netherlands*
‡ *Electron Microscopy for Materials Research (EMAT), University of Antwerp, Groenenborgerlaan 171, 2020 Antwerp, Belgium*

* E-mail: W.Albrecht@uu.nl; A.vanBlaaderen@uu.nl

Methods

Gold nanorods were synthesized following the method of Ye et al.[1]. The average aspect ratio and volume of the rods were 3.5 ± 0.5 and (9.9 ± 0.4)· 10^4 nm^3, respectively. The rods were then coated with a 14 nm thick mesoporous silica shell following the method of Gorelikov and Matsuura[2]. The coated particles were stored in ethanol. Shell thickness and particle sizes and the polydispersity were determined by analyzing TEM images of about 330 particles.

In order to achieve local single particle laser-induced heating a Leica SP8 confocal setup (63x/1.4 oil-immersion confocal Leica objective) equipped with both, a Coherent chameleon II Ti:Sapphire laser (80 MHz repetition rate, 140 fs pulse length) and a fiber-based white light laser, was used. For the laser-induced deformations, a drop of the particle dispersion was dropcasted on a TEM finder grid. TEM images of all particles in a spot of about 12 μm × 12 μm were taken with a TECNAI12 electron microscope. The grid was then placed on a microscopy slide. Subsequently, glycerol was put on top of the grid to reduce the scattering of the silica (refractive index of 1.45), while also being close to the index of the immersion oil and glass (refractive index of 1.51). This sample system was then closed with a 0.1 mm thick cover glass. The white light laser at the 480 nm laser line was used in reflection mode to find back the spot which was looked at by the TEM before and to focus onto the right z-plane. For the laser-induced heating a thin 3D stack with 2D planes of 11.5 μm × 11.5 μm was scanned by the Ti:Sapphire laser at 860 nm with a pixel size of 22.6 nm × 22.6 nm and a pixel dwell time of 1.2 μs (400 Hz scanning speed). From those values we estimate that roughly 2·10^4 pulses are incident per nanorod. The simulated axial and longitudinal point spread functions for this specific setup can be found below. After illumination the glycerol was removed by drying the TEM grid in vacuum overnight. The particles of the same spot were imaged in the TEM afterwards. This enabled us to study the heat-induced deformation on a single particle level and to analyze the same particles before and after deformation. The method is illustrated in Figure 1a. The time-averaged laser power was measured by a Thorlabs PM200 powermeter using a Thorlabs S170C microscope slide power sensor.

EELS measurements were performed on a monochromated aberration-corrected microscope operated at 120 kV. Using a monochromator, an energy resolution of 150 meV was obtained as measured by the width at half maximum of the zero loss peak. For the acquisition of the plasmon maps, a pixel size of 1.3 nm is used with a spectrum collection time of 0.03 s.In order to analyze the recorded EELS data cubes, a power law background subtraction was performed using Digital Micrograph 2.3.0. Plasmon maps are then obtained using an energy selecting window that is positioned at the desired energy losses corresponding to the different plasmon modes. The FDTD simulations were performed with the software FDTD solutions 8.12.590 from Lumerical Solutions. We used the dimensions as measured by TEM after deformation for particle 1 in Figure 2b and a mesh size of 0.5 nm.

Measured and calculated extinction spectra

The silica-coated gold nanorods were stored in ethanol where they exhibit a longitudinal plasmon peak position at 828 nm (Figure S1a black solid curve). After sandwiching the dried particles between a microscopy slide and a 0.1 mm thick cover glass with glycerol in between the spectrum red-shifts to 860 nm due to the higher surrounding refractive index (Figure S1a red solid curve). For calculating the extinction spectra with Mie-Gans theory, which only has an analytical solution for particles with a spheroidal shape, we used the corresponding shape factors that were determined phenomenologically in Ref.[3]. ϵ_1 and ϵ_2 were taken from Olmon et al.[4]. The peak positions of the spectrum measured in ethanol, glycerol and vacuum can be reproduced by using a dielectric constant of the surrounding of 1.86 (black dashed curve), 2.06 (red dashed curve) and 1.7 (dashed blue curve) which are reasonable values. We assume that the effects of a small jump in refractive index at the silica-glycerol interface to be negligible especially as the silica is also porous. Figure S1b compares the calculated peak positions of the original (average) nanorod (black curve) to the measured reduced average aspect ratio after illuminating with 5.3 mJ/cm^2 (aspect ratio of 3.0). The thicker diameter in the case of the deformed particle is taken into account by the corresponding shape factors from Prescott et al.[3]. This approximation leads to a peak shift of 25 nm in glycerol which will shift it out of the excitation wavelength of the laser. This calculated shift can only be seen as an indication as other factors also influence the peak shift such as heating of the surrounding glycerol resulting in a change of its dielectric constant and polydispersity[3].

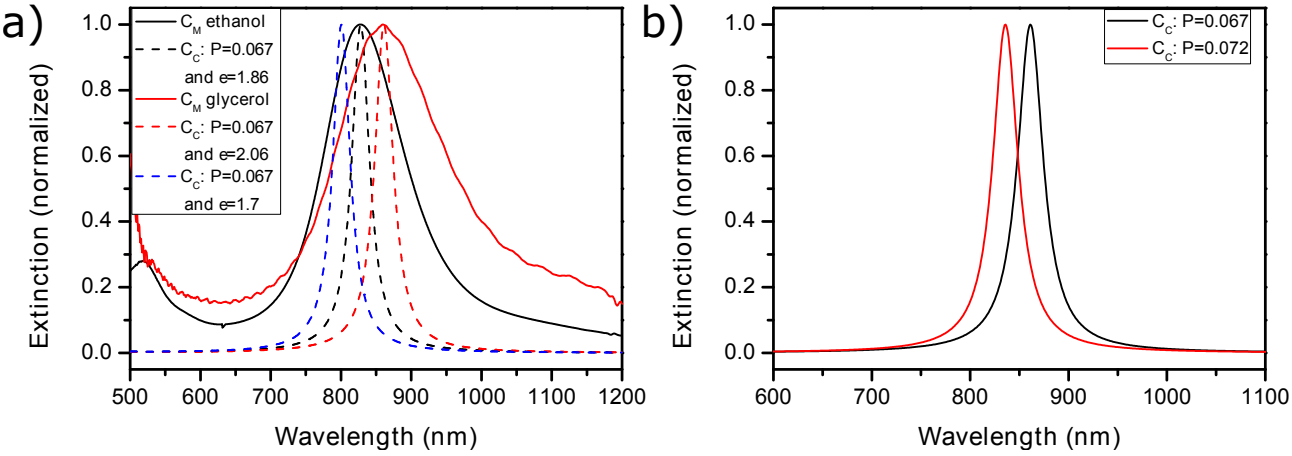

Figure S1: a) The black curve shows the extinction of the mesoporous silica-coated gold nanorods in ethanol. The extinction in glycerol (red curve) is red-shifted by 30 nm due to a higher dielectric constant. The black, red and blue dashed curves were produced by Mie-Gans theory with the shape factors presented in[3] and an ϵ_d of 1.86, 2.06 and 1.7, respectively. b) compares the calculated peak positions of an average nanorod before (black curve) and after an illumination of 5.3 mJ/cm^2.

Heat dissipation times

Heat dissipation times τ_d for our system and for comparison for the system in Ref.[5] are estimated by using the relationship: $\tau_d \propto R^2/(\rho_s C_s \Lambda_s)$ where R is the radius of the gold particle and ρ_s, C_s and Λ_s are the density, the heat capacity and the thermal conductivity of the surrounding medium, respectively. Hu et al. measured a heat dissipation time τ_d^{ref} for a 15 nm sized gold particle with a 10 nm thick Stoeber silica shell of 100 ps in ethanol[6]. The heat dissipation time of our system τ_d can then be estimated by

$$\frac{\tau_d}{\tau_d^{ref}} = \frac{R}{R^{ref}} \frac{\rho_s^{ref} C_s^{ref} \Lambda_s^{ref}}{\rho_s C_s \Lambda_s}. \quad (1)$$

The parameters ρ_s^{ref}, C_s^{ref} and Λ_s^{ref} are taken for a composite system of Stoeber silica and ethanol with a silica porosity of 13%[7]. For our system we assume a composite system of mesoporous silica and glycerol with a silica porosity of 70%[8]. ρ_s, C_s and Λ_s for ethanol, silica and glycerol were taken from[9]. Based on those assumptions we estimate a heat dissipation time of 500 ps for our system. The gold nanorods in[5] are embedded in a poly vinyl alcohol matrix. The corresponding parameters are taken from[10] and τ_d can be estimated to be 2000 ps. It needs to be mentioned that the thermal conductivity at the interface between the gold and the

surrounding medium is neglected here since for gold particles with a diameter above roughly 10 nm the cooling rate is dominated by heat diffusion into the surrounding medium[6].

Confocal point spread functions

The lateral and axial point spread functions of our confocal setup (Leica SP8 using a 63x/1.4 oil-immersion confocal Leica objective) were simulated with the Huygens software for an excitation wavelength of 860 nm and glycerol as a medium. The point spread functions have recently been measured for such a setup for an excitation wavelength of 488 nm and 543 nm[11] and were in good agreement with the simulated ones (not shown here). Since the point spread functions depend on excitation wavelength and surrounding medium we did not use the measured values but simulated them for an excitation wavelength of 860 nm and glycerol as a medium. The extracted profiles are presented in Figure S2a. The full width at half maximum (FWHM) of the lateral profile is 319 nm which determines the radius of the spot size and was used to calculated the fluences. For estimating the intensity drop below or above the focal plane we simulated the axial point spread function in the x-z plane and extracted profiles in the focal plane and 240 nm above. By comparing the area under the profile in the focal plane and 240 nm above the focal plane we calculate an intensity drop to 70%.

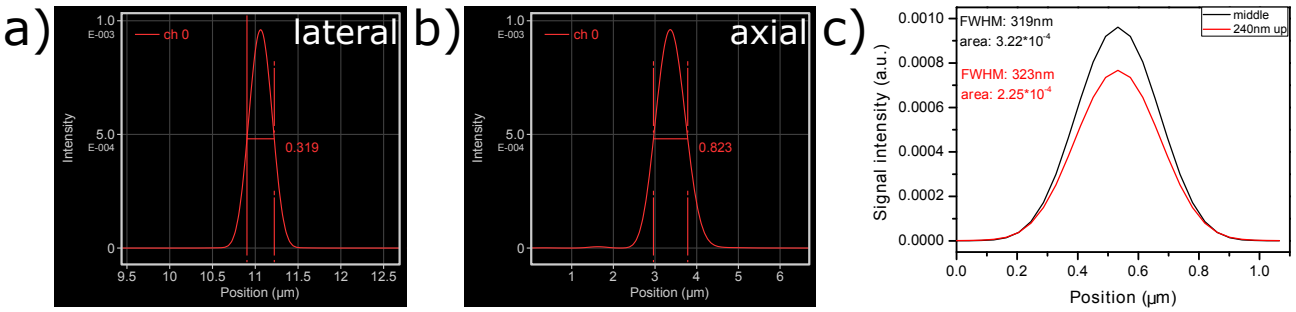

Figure S2: a) and b) show the lateral and axial profile of the point spread function with their FWHM, respectively. c) shows the lateral extracted spectra at the middle (black) and 240 nm above the middle (red) of the axial point spread function.

FDTD simulations for particle 1 in Figure 2

Representative FDTD simulations were performed for one intermediate particle shape in vacuum (particle 1 in Figure 2b). The obtained longitudinal and transverse plasmon resonances were at 694 nm (1.79 eV) and 514 nm (2.41 eV), respectively, which are in very good agreement with the measurements (1.8 eV and 2.4 eV for the longitudinal and transverse resonance, respectively). The corresponding plasmon map for the longitudinal resonance is shown in Figure S3.

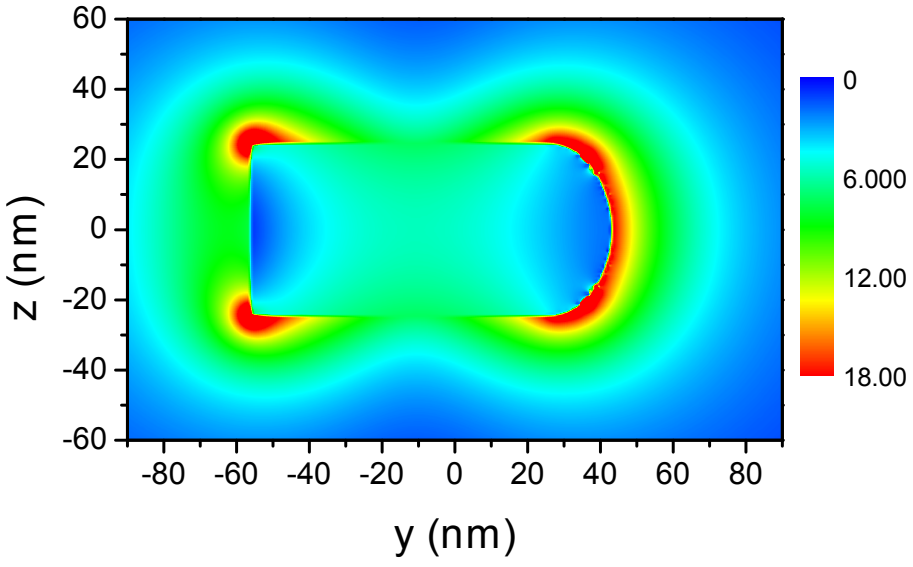

Figure S3: Longitudinal plasmonic field enhancement from FDTD simulations for the rod in Figure 2b.

Au nanorod size reduction and analysis of clusters

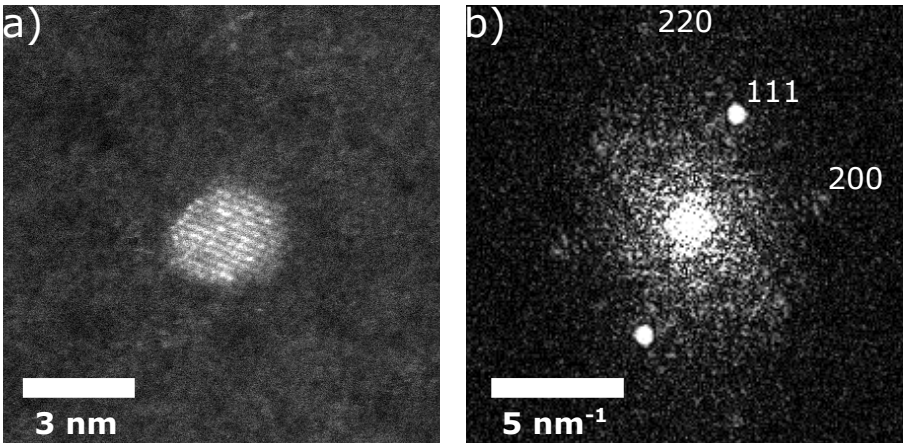

Figure S4: a) shows a high-resolution STEM image of a small gold cluster. b) shows the FFT of the particle in a).

Table S1: Ratios and differences of the measured lattice spacings are compared to the calculated ones. The ratios are dimensionless and the differences are displayed in nm.

	d_{111}/d_{200}	d_{111}/d_{220}	d_{200}/d_{220}	$d_{111}-d_{200}$	$d_{111}-d_{220}$	$d_{200}-d_{220}$
measured	1.158	1.692	1.462	0.030	0.090	0.060
calculated	1.155	1.633	1.414	0.032	0.091	0.059

A high-resolution STEM image of clusters that were observed close to some Au nanorods after fs-laser irradiation at higher fluences is shown in Figure S4a. The cluster is crystalline and the corresponding fast Fourier transform (FFT) is shown in 4b). The measured lattice spacings d_{111}, d_{200} and d_{220} are 0.22 nm, 0.19 nm and 0.13 nm, respectively. Calculated lattice spacings for the known lattice constant of 0.40786 nm are 0.2355 nm, 0.2039 nm and 0.1442 nm. The measured spacings are a bit smaller since the lattice constant of gold decreases with decreasing cluster size[12]. That we see the three lattice spacings d_{111}, d_{200} and d_{220} can be confirmed by calculating the ratios of the three values and comparing them to the calculated values as shown in Table S1. Furthermore, by taking the difference between the three values and comparing them to the calculated ones it can be confirmed that the clusters are gold (Table S1). It is worth mentioning that the clusters did not neccessarily penetrate through the shell as a whole but they could also be in forms of ions and enter in an oxidized form the glycerol forming clusters there and finally precipitating after drying.

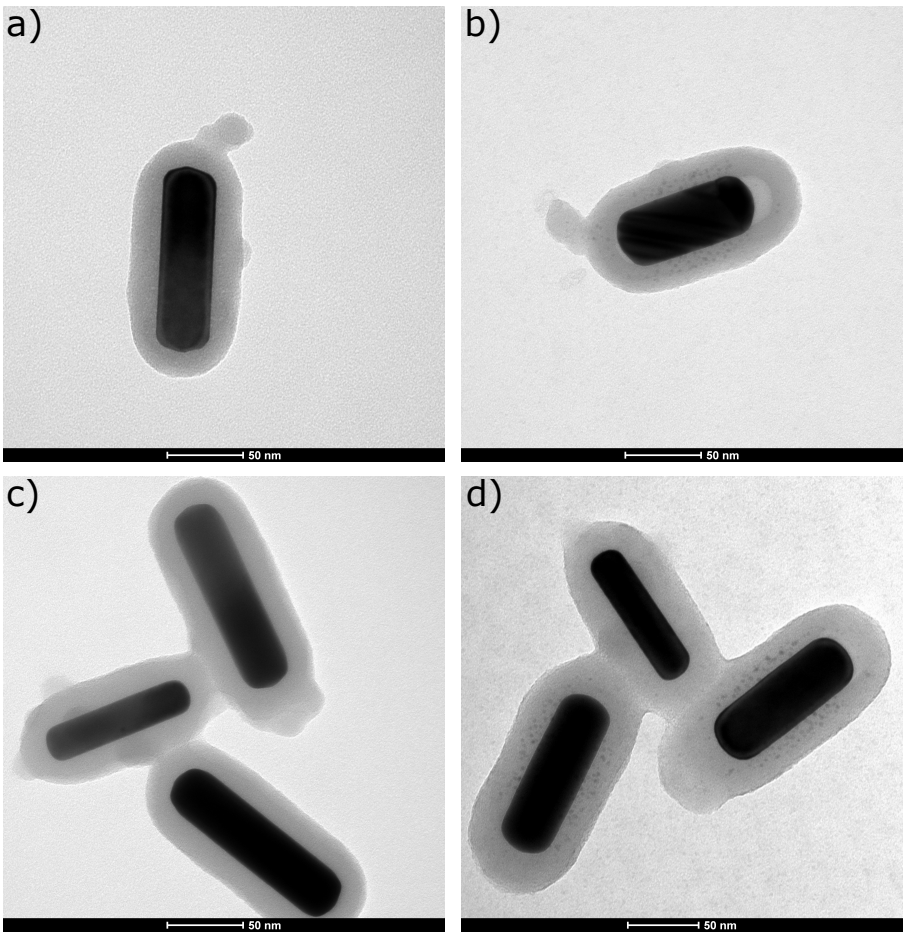

Figure S5: a) and b) show two examples of small gold fragments that got stuck in a denser shell. A thin layer of Stoeber silica was coated around the mesoporous shell resulting in a total shell thickness of 18 nm. From etching experiments we know that such a layer closes off the pores[13].

References

[1] Ye, X.; Zheng, C.; Chen, J.; Gao, Y.; Murray, C. B. *Nano Lett.* **2013**, *13*, 765–771.

[2] Gorelikov, I.; Matsuura, N. *Nano Lett.* **2008**, *8*, 369–73.

[3] Prescott, S. W.; Mulvaney, P. *J. Appl. Phys.* **2006**, *99*, 123504.

[4] Olmon, R. L.; Slovick, B.; Johnson, T. W.; Shelton, D.; Oh, S. H.; Boreman, G. D.; Raschke, M. B. *Phys. Rev. B* **2012**, *86*, 235147.

[5] Zijlstra, P.; Chon, J. W. M.; Gu, M. *Phys. Chem. Chem. Phys.* **2009**, *11*, 5915–5921.

[6] Hu, M.; Wang, X.; Hartland, G. V.; Salgueiriño Maceira, V.; Liz-Marzán, L. M. *Chem. Phys. Lett.* **2003**, *372*, 767–772.

[7] Bogush, G.; Tracy, M.; Zukoski, C. *J. Non. Cryst. Solids* **1988**, *104*, 95–106.

[8] Kierys, A.; Buda, W.; Goworek, J. *J. Porous Mater.* **2010**, *17*, 669–676.

[9] Haynes, W. In *CRC Handbook of Chemistry and Physics*, 96th ed.; Haynes, W., Ed.; CRC: Boca Raton, 2015.

[10] Ellis, B.; Smith, R. In *Chromatographia*, 2nd ed.; Ellis, B., Smith, R., Eds.; CRC: Boca Raton, 2010.

[11] Besseling, T. H.; Jose, J.; van Blaaderen, A. *J. Microsc.* **2015**, *257*, 142–150.

[12] Qi, W. H.; Wang, M. P. *J. Nanoparticle Res.* **2005**, *7*, 51–57.

[13] Deng, T.-S.; van der Hoeven, J. E. S.; Yalcin, A. O.; Zandbergen, H. W.; van Huis, M. A.; van Blaaderen, A. *Chem. Mater.* **2015**, *27*, 7196–7203.